Influence of elastic variations on crack initiation in functionally graded glass-filled epoxy

Carl-Ernst Rousseau [1], Hareesh V. Tippur [*]

Department of Mechanical Engineering, Auburn University, 202 Ross Hall, Auburn, AL 36849, USA

Abstract

Crack tip deformations and fracture parameters in functionally graded glass-filled epoxy beams are experimentally evaluated under static and dynamic loading conditions. Beams with unidirectional, monotonic elastic gradients and cracks along the gradient are examined. SEN samples with increasing or decreasing Young's modulus ahead of the crack tip are studied in symmetric four-point bending and one-point impact loading configurations. Optical method of coherent gradient sensing (CGS) is used to measure crack tip deformations prior to crack initiation. For impact loading experiments, CGS is used in conjunction with high-speed photography for recording instantaneous deformation fields. Stress intensity factors (SIF) or SIF-histories in functionally graded materials (FGM) based on locally homogeneous material descriptions in the immediate crack tip vicinity are evaluated and compared with companion finite element simulations. The influence of elastic gradients in FGM samples with cracks on the compliant and stiff sides of the beam are quantified relative to their homogeneous counterparts and with each other. Under static loading conditions, the crack tip located on the compliant side of the beam is elastically shielded when compared to the situation when the crack is on the stiffer side of the same FGM beam. Under dynamic conditions, however, elastic gradients affect crack initiation differently. Crack initiation in an FGM with a crack on the stiff side of the beam and impact occurring on the compliant edge is delayed when compared to the opposite configuration. Independent finite element simulations of FGMs with idealized elastic gradients with identical crack tip elastic properties suggest that lower crack tip loading rate in the former is responsible for the differences.
© 2002 Elsevier Science Ltd. All rights reserved.

1. Introduction

Nonhomogeneous material systems with gradual variation in properties are collectively referred to as functionally graded materials or FGMs. Gradual variation of material properties in FGMs, unlike abrupt

---

[*] Corresponding author. Tel.: +1-334-844-3327; fax: +1-334-844-3307.

E-mail address: htippur@eng.auburn.edu (H.V. Tippur).

[1] Present address: California Institute of Technology, Pasadena, CA.

changes encountered in discretely layered systems, is known to improve failure performance [1] while preserving the intended thermal, tribological, and/or structural benefits of combining dissimilar materials. Accordingly, FGMs are considered ideal for applications involving high strain rate and thermal shock loading. Assessing the influence of compositional and hence material property gradients on the failure behavior is central for understanding FGMs. In this article, the influence of elastic gradients on the static and dynamic crack initiation in FGMs is examined. *Of specific interest to this work are FGMs with cracks parallel to the elastic gradient*.

Some of the early works on the fracture mechanics of FGMs include those by Atkinson and List [2], and Delale and Erdogan [3]. An inverse $\sqrt{r}$ stress singularity at the crack in FGMs was suggested in these articles and was later confirmed by Eischen [4] using asymptotic analysis. Jin and Noda [5] concluded likewise, independently of the crack orientation relative to the property gradient. In a paper summarizing recent advances in fracture mechanics of FGMs, Erdogan [6] has presented theoretical results for cracks oriented along the elastic gradient, and subjected to various loading conditions. Among the dynamic investigations on FGMs, transient (stress intensity factor) SIFs for a mode-III crack lying in an elastic media with spatially varying elastic properties normal to crack surfaces has been studied analytically by Babaei and Lukasiewicz [7]. They have found SIF to vary with crack length to layer thickness ratio. Dynamic crack propagation in functionally graded particulate is numerically studied by Nakagaki et al. [8] for shock loading to determine the effect of grading on crack severity as the crack propagates in the FGM. Parameswaran and Shukla [9] have shown experimentally that increasing toughness in the direction of crack growth reduces crack jump distance in discretely layered FGMs. Chiu and Erdogan [10] have evaluated the effect of material nonhomogeneity on one-dimensional wave propagation in FGMs having gradation in the direction of the incident pulse. Considerable wave distortions are reported as a rectangular pressure pulse propagates in the material.

Among the few experimental mechanics investigations on FGMs reported to date, Marur and Tippur [11] have developed an elastic impact method for characterizing the elastic properties of glass-filled epoxy FGMs. FGM processing, characterization and optical evaluation of SIFs are reported by Butcher et al. [12]. They have studied an FGM with a crack normal to the direction of the compositional gradient and observed enhancement of crack initiation toughness in graded systems when compared to bimaterials. A particulate FGM made of cenospheres dispersed in polyester matrix has been developed by Parameswaran and Shukla [13]. A UV-irradiated polymeric FGM has been prepared by Li et al. [14] to study quasi-static crack growth along the elastic and fracture toughness gradients. Boundary value measurements are used in finite element simulations to demonstrate toughening behavior of the FGM relative to homogeneous materials when the crack propagated from the stiffer side to compliant side. Finally, Marur and Tippur [15] have performed strain gage measurements and finite element simulations to evaluate dynamic performance of graded interface having cracks normal to the elastic gradient with respect to those of bimaterial. They have measured lower rate of crack tip loading in FGMs compared to the bimaterial counterparts.

In the present study, a comparative study of the influence of unidirectional elastic variations on crack initiation in FGMs subjected to static loading and low velocity impact is provided. FGMs with cracks oriented along the direction of the elastic gradient are considered. Although local fracture toughness dominantly affects crack initiation and growth in FGMs, there are instances [13,16] where material processing issues (resulting in porosity and other microdefects) could result in a relatively constant fracture toughness with monotonically varying elastic properties. Accordingly, attention is focussed on isolating the influence of elastic gradient on crack initiation in this paper. Following this introduction, a brief background of the elastic crack tip fields for FGMs is given. Section 3 describes material characteristics, optical technique and the method of extraction of the SIFs. Section 4 provides details of the complementary numerical simulations performed in this study. Finally, Section 5 summarizes the results for both static and dynamic experiments.

2. Elastic crack tip fields in FGMs: continuum models

For a crack oriented along the direction of the elastic gradient in a nonhomogeneous, isotropic planar body, using asymptotic analysis, Eischen [4] has shown that the crack tip stresses, say sum of the in-plane normal stresses $(\sigma_x + \sigma_y)$, in an FGM for mode-I conditions can be expressed as,

$$(\sigma_x + \sigma_y) = (C_0 r^{-1/2} f_0^{\mathrm{I}}(\theta) + C_1 r^0 f_1^{\mathrm{I}}(\theta)) + \mathrm{O}(r^{1/2}), \tag{1}$$

where (r, θ) denote crack tip polar coordinates, f_0^{I}, f_1^{I} are angular functions, and C_0 and C_1 are the coefficients of the expansion with $C_0 = K_{\mathrm{I}}/\sqrt{2\pi}$, K_{I} being the mode-I SIF. The angular functions have been shown to be identical to the ones for a crack in a homogeneous body. Accordingly, stress field description is identical to the homogeneous counterpart for the first two terms of the expansion. Moreover, Rousseau [17] has determined experimentally that addition of an expression of the form $C_2 r^{1/2} f_2^{\mathrm{I}}(\theta)$ can be used adequately as a third term in the asymptotic expansion, where C_2 is an unknown coefficient, and f_2^{I} is defined as the same angular function used for homogeneous materials. Expressions for in-plane displacements in FGMs were also developed by Eischen [4]. It was found that asymptotic displacement terms proportional to $r^{1/2}$, r^0 and r^1 are identical to those of homogeneous materials, thus are independent of gradient. The experimental method used in the current study measures surface slopes, and hence expressions for out-of-plane displacements, w, are necessary. Assuming plane stress conditions and constant thickness-wise strain, out-of-plane displacement can be obtained as,

$$w \approx \frac{-vB}{2} (A_0 r^{-1/2} f_0^{\mathrm{I}}(\theta) + A_1 r^0 f_1^{\mathrm{I}}(\theta) + A_2 r^{1/2} f_2^{\mathrm{I}}(\theta)) + \mathrm{O}(r), \tag{2}$$

with $A_j = C_j/E_0$ where the subscript E_0 denotes the value of crack tip Young's modulus. In the above, the Poisson's ratio v is assumed to be constant in the FGM.

Near tip expressions for stress fields in nonhomogeneous planar bodies that include the influence of elastic property gradients are reported by Erdogan [6]. For an exponential variation of elastic modulus of the form,

$$E(x) = E_0 \mathrm{e}^{\alpha x} = E_0 \mathrm{e}^{r\alpha\cos\theta}, \tag{3}$$

where E_0 is the Young's modulus at the origin, and α is a scalar dependent on the terminal values of the modulus and the length of the graded region, the near tip mode-I stresses are shown to be of the form,

$$\sigma_{ij}(r, \theta) \cong \mathrm{e}^{r\alpha\cos\theta} \left(\frac{K_{\mathrm{I}}}{\sqrt{2\pi r}} f_{ij}^{\mathrm{I}}(\theta) \right), \quad (i, j = x, y). \tag{4}$$

As $r \to 0$, Eq. (4) reduces to the K-dominant terms of Eq. (2).

In the absence of explicit expressions for stress fields for dynamically loaded stationary cracks, it could be inferred that Eq. (2) could be adequately extended for dynamic cases where inertial effects enter the coefficients without modifying the overall form of the expressions (i.e., $A_i \equiv A_i(t)$).

3. Experiments

3.1. The material and its elastic characteristics

Compositionally graded samples used in the current research comprised of an epoxy matrix (Young's modulus ~ 3 GPa, Poisson's ratio ~ 0.35) in which varying quantities of solid A-glass spheres (mean diameter ~ 42 μm) were dispersed. Thus the composite is *microscopically heterogeneous* but will be treated as
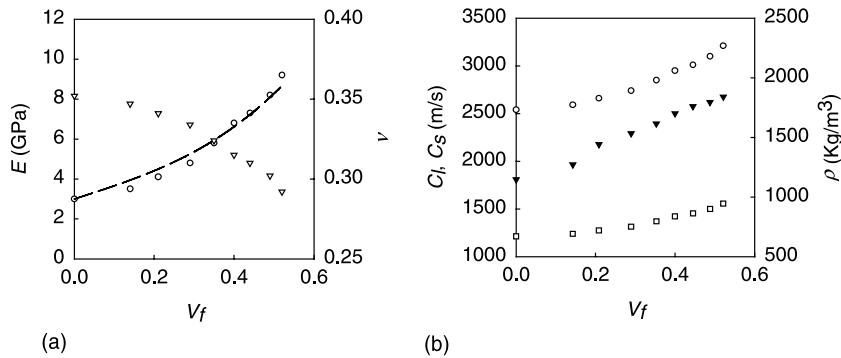
Fig. 1. Material properties of glass-filled epoxy particulate composites: (a) static Young's modulus and Poisson's ratio with filler volume fraction, (b) wave speeds and density with filler volume fraction.

an *isotropic, nonhomogeneous material at macroscopic scales* for measurement and analysis using continuum models. (That is, the material characteristics and optical measurements, to be discussed, are averaged over length scales that are 1–2 order of magnitude larger than the mean particle size.)

Prior to discussing the material properties of the FGMs used in the experiments, properties of homogeneous particulate glass-epoxy composites with different volume fraction of filler are described. Fig. 1(a) shows measured Young's modulus and Poisson's ratio variation of macroscopically *homogeneous mixtures* having different but constant volume fractions of the filler in the matrix. Young's modulus from about 3 to 9 GPa (static conditions) and a Poisson's ratio variation from 0.35 to 0.29 when the volume fraction of the filler is increased from 0 to 0.5. Also included in the figure are micromechanics predictions of the elastic modulus for two-phase mixtures [18] for different volume fractions V_f. Evidently, the predictions follow the experimental measurements rather closely over the entire range of filler volume fractions. (It should also be noted that these particle filled compositions show a linear load–displacement behavior [12] and can be treated to be nominally linear elastic.) In Fig. 1(b), the dynamic material properties namely longitudinal and shear wave speeds and density of the composites are shown. Evidently, each of these properties increases monotonically with the filler volume fraction in the composite.

Gravity casting was used for producing FGMs with monotonic Young's modulus variation between approximately 3 and 9 GPa under static conditions (measured using cantilever beam tests) or, approximately 4–12 GPa, under dynamic conditions (measured using ultrasonic pulse-echo measurements). These values of Young's moduli correspond to that of pure epoxy and a composite with a volume fraction of glass spheres in an epoxy matrix of ∼0.5, respectively. Details of the methods used in determining the elastic characteristics can be found in Butcher et al. [12]. Fig. 2 shows the modulus variation in a typical FGM sheet. The graded region in these sheets were machined into beam samples (dimensions 120 mm × 20 mm × 6 mm for static experiments and 150 mm × 37 mm × 6 mm for dynamic experiments). Fig. 2 shows typical elastic variation in a casting of which a portion was machined to obtain beam samples having the necessary elastic properties. The sample surfaces were then deposited with a thin layer of aluminum to obtain specular surface necessary for optical measurements. Edge notches (root radius 75 μm and length of 6 mm) were cut into the samples using a high-speed diamond impregnated circular saw.

Homogeneous samples (without compositional gradients) having elastic moduli equal to the ones at the crack tips of the FGMs were also prepared for comparative study. The geometry of these homogeneous samples was identical to that of the FGM samples.
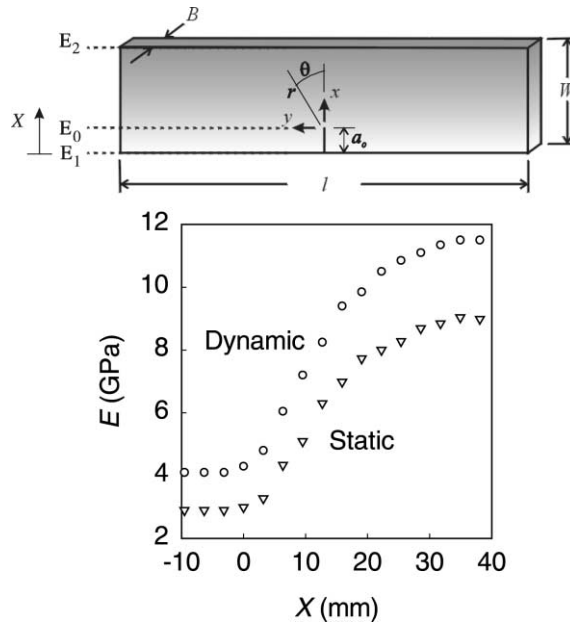
Fig. 2. Typical Young's modulus variations in cast FGM sheets.

3.2. Optical technique: coherent gradient sensing

The optical method of *reflection* coherent gradient sensing (CGS) was used for measuring crack tip deformations. The working principle of CGS has been reported by Tippur et al. [19]. An expanded and collimated beam of laser light (typically 50 mm in diameter) was used to interrogate the *specular* surface of the specimen. The reflected light beam, or the object wave front, contained information about the surface deformations. Optical shearing of the object wave front was used to decipher surface deformations in the form of interference patterns representing contours of constant surface slopes. In the present work, surface slopes along the crack orientation (x-axis) were determined as,

$$\frac{\partial w}{\partial x} = \frac{Np}{2\Delta}, \quad N = 0, \pm 1, \pm 2, \ldots, \tag{5}$$

where N denotes fringe orders, p is the pitch of the gratings (25 μm), and Δ is the grating separation distance. For plane stress conditions, the out-of-plane displacement w can be related to the in-plane stress components using expression for average out-of-plane strain, $\varepsilon_z \cong 2w/B$, or,

$$w \cong -\frac{vB}{2}\left(\frac{\sigma_x + \sigma_y}{E}\right), \tag{6}$$

where B is the undeformed thickness of the sample.

Interference fringes were recorded in real-time using a conventional camera during static experiments. The experimental set-up for dynamic study, however, was more elaborate. It included an impactor for stress wave loading, a pulse-laser as a light source, a CGS interferometer and a continuous access high-speed camera. During the experiment, a pneumatically operated impactor with a steel cylindrical head was launched towards the specimen. During its descent, the hammer first triggered open an electronic shutter of the high speed rotating mirror camera pre-spun to the desired speed, allowing light to reach its internal cavity. The specimen was subjected to one-point symmetric impact. An adhesive-backed copper tape placed

on the top edge of the beam closed an electric circuit when contacted by the hammer. This in turn triggered the laser to begin pulsing at a repetition rate of 5 μs, with a pulse width of 50 ns, for a time duration of less than or equal to a single sweep of the light beam on the stationary film track of the high-speed camera.

3.3. Optical measurements

3.3.1. Statically loaded stationary cracks

The FGM and homogeneous beam samples were quasi-statically loaded in four-point bending using an Instron-4465 machine in displacement control mode (cross-head speed ∼ 0.25 mm/min). The samples were subjected to symmetric bending moment acting over a 60 mm length in the mid-span of each beam. The resulting crack tip fringe patterns in FGMs with a crack on the stiff ($E_2/E_1 < 1$) and the compliant sides ($E_2/E_1 > 1$) of the beam are shown in Fig. 3(a) and (c), respectively. In these cases, the crack tip Young's moduli were 6.8 and 4.8 GPa, respectively. Further, the far-field applied stress σ_∞ ($= 6M/BW^2$ where M is the moment, W and B are the beam height and thickness, respectively) at which the deformations were recorded in the two cases are the same. Homogeneous samples having crack tip Young's moduli same as (to within ±3%) that of the FGMs were also optically investigated. The crack tip deformation patterns for the homogeneous beams corresponding to the FGMs with the crack on the stiff and compliant side are shown in Fig. 3(b) and (d), respectively. Note that, the fringe patterns from the homogeneous samples are for the same load level as their FGM counterparts. The sensitivity of the optical measurements is ∼0.015°/fringe. In each case, the fringes are nominally symmetric about the crack plane indicating mode-I behavior. However, qualitative differences exist between the fringe patterns in terms of relative fringe sizes between
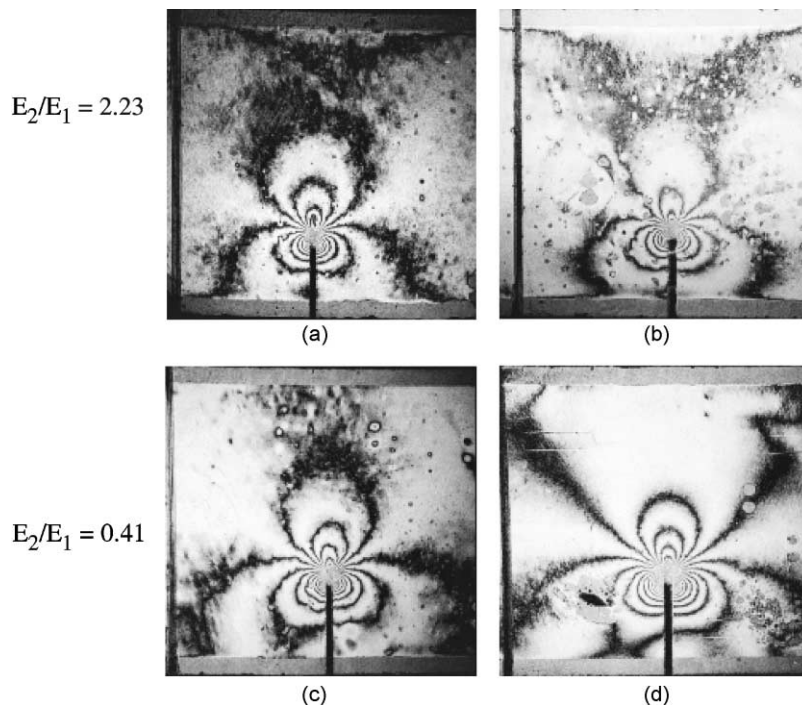

Fig. 3. Crack tip interference representing $\delta w/\delta x$ contours for a far-field bending stress $6M/BW^2 = 10.2$ MPa: (a) FGM with $E_2/E_1 = 0.41$, (b) homogeneous counterpart of (a), (c) FGM with $E_2/E_1 = 2.23$, (d) homogeneous counterpart of (c) (center-to-center distance from crack to drawn line is approximately 10 mm).

front and rear crack tip lobes in FGMs and, between the ones in FGMs and the equivalent homogeneous beams. These differences were quantified by extracting crack tip SIFs from the fringe patterns.

3.3.2. Dynamically loaded stationary cracks

The FGM and homogeneous beam samples were impact loaded in one-point symmetric loading configuration with a velocity of 5.3 m/s. The resulting interference patterns representing contours of dw/dx were recorded at a rate of 200 000 frames/s. For brevity, two select interferograms are shown for each experiment, at times 25 and 75 μs after impact, the latter being close to crack initiation in each case. CGS fringes for the homogeneous material are shown in the first column of Fig. 4. Fringes for the FGMs with crack located on compliant and stiff sides of the gradient are shown in the second and third columns of Fig. 4, respectively. The homogeneous beam had a uniform volume fraction of 0.42, and an elastic modulus of 9.6 GPa. The FGM with crack on the compliant side ($E_2/E_1 \sim 2.9$) has elastic modulus variation between 4 and 11 GPa with a value of $E_0 \sim 5.6$ GPa at the crack tip. Terminal values of Young's moduli are nearly the same for the FGM with crack on the stiff side ($E_2/E_1 \sim 0.45$), with crack tip $E_0 \sim 10$ GPa.

The structure of the fringe patterns in the crack tip vicinity for the two FGMs qualitatively resemble those in the homogeneous material. At the crack tip, one set of frontal and two sets of equally prominent lateral fringe lobes are present. Further examination of crack tip fringes in the FGM with crack on the compliant side ($E_2/E_1 > 1$, Fig. 4) show some deviation relative to the homogeneous case. Crack tip fringe lobes ahead of the crack show a lateral spread normal to impact direction. In this case, the compressive stress waves progressively slow down as they encounter more compliant material when they propagate away from the stiff edge. The opposite occurs when the tensile waves are reflected from the cracked edge.
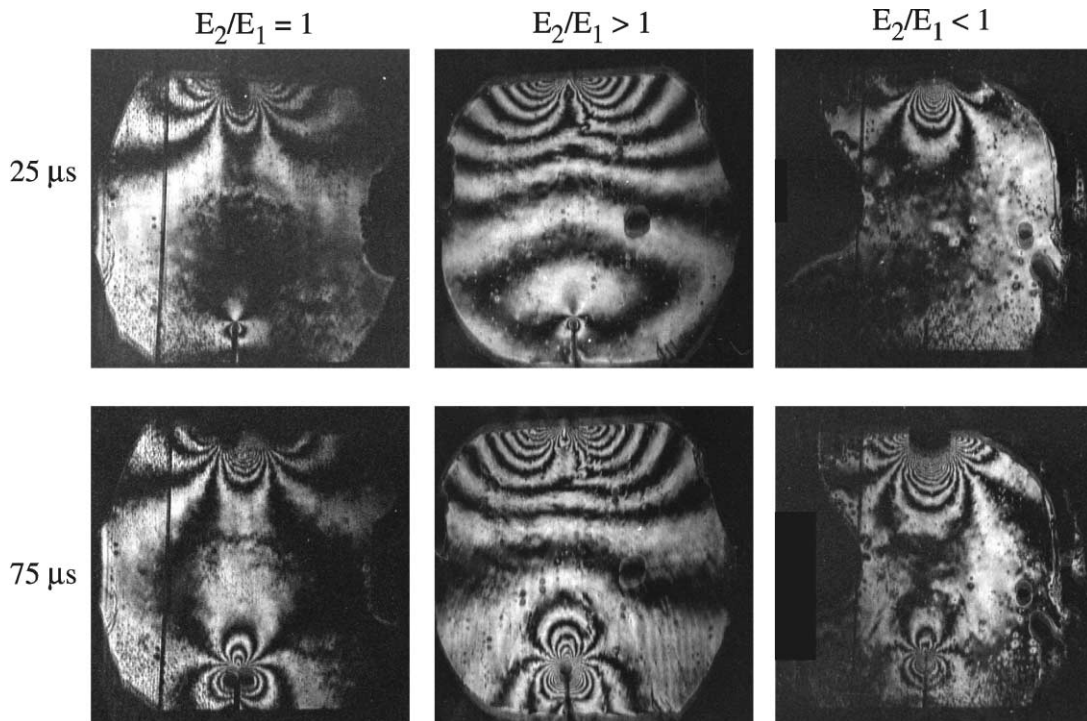

Fig. 4. Representative crack tip interference representing surface slope $\delta w/\delta x$ contours for homogeneous and FGM samples (fringe sensitivity 0.015°/fringes).

Crack tip fringes for the FGM with crack on the stiff side ($E_2/E_1 < 1$, Fig. 4) have a similar appearance to those for the homogeneous material. Here, the compressive stress waves generated at the compliant edge progressively encounter stiffer material and hence speed up during propagation away from the compliant edge. Nearly equi-sized front and rear fringe lobes around the crack tip are present. Additionally, a relatively uniform far-field is evident in this specimen.

For the homogeneous sample ($E_2/E_1 = 1$) with a longitudinal velocity of $\sim$2980 m/s, approximately 12.5 µs are required for the initial compressive waves to reach the bottom edge of the beam. The reflected tensile waves load the crack tip $\sim$ 15 µs after impact. Following that, crack tip fringes progressively enlarge and become more numerous up to crack initiation at $\sim$85 µs. Average longitudinal wave speed $(\overline{C}_l = 1/W \int_{-a}^{W-a} C_l(x)\,\mathrm{d}x)$ for the FGM specimen with crack on the compliant side ($E_2/E_1 > 1$) is $\sim$2910 m/s. In this case, initial propagation times of compressive and reflected tensile waves are similar to those of the homogeneous material. It is important to remember here that compressive waves progressively slow down as the crack tip is approached while the opposite is true for reflected tensile waves. The crack initiates $\sim$80 µs after impact. The FGM with the crack on the stiff side ($E_2/E_1 < 1$) has an average longitudinal velocity of $\sim$2900 m/s over the height of the beam. Again, this velocity corresponds to times of $\sim$12.5 µs for a compressive wave to reach the bottom edge, and $\sim$2.5 µs for a tensile wave to reflect to the crack tip. In this case, the incoming compressive waves from the contact point travel progressively faster towards the crack tip while the reverse occurs for the reflected tensile waves. The size of the crack tip fringes increases gradually until initiation at about 90 µs. An observation pertinent to FGM and homogeneous specimens can be made: compressive and tensile waves arrive at the original crack tips at approximately the same times for all the specimens since the average longitudinal wave speeds are nearly same. Therefore, initial crack tip loading occurs at nearly the same time. Local properties at individual crack tips, as well as nonuniform wave reflections from the edges will contribute to varying conditions in crack initiation between the different specimens. Evidently, the crack in the FGM with $E_2/E_1 < 1$ experiences delayed crack initiation relative to the one with $E_2/E_1 > 1$.

3.3.3. Extraction of SIFs from interferograms

Overdeterministic least-squares analyses of optical data [19] were used for extracting instantaneous SIFs. Briefly, the method consisted of digitizing the interferograms around the crack tip to obtain fringe order N and location (r, θ) data. In view of 3-D effects in the immediate crack tip vicinity, optical data within $r/B < 0.4$ were not considered in the analysis. This was based on existing knowledge of crack tip field triaxiality in finite size homogeneous samples [20]. Further, for mode-I, it has been shown using CGS that [19], data in the sector $90° < |\theta| < 135°$ have the least amount of 3-D effects and closely follow plane stress behavior. (Similar conclusions have been drawn in case of bimaterial interfacial cracks in finite thickness samples as well [21].) Also, a difference representation of Eq. (5) was used for least-squares data analysis, by minimizing the least-squares error $((\delta w/\delta x) - (Np/2\varDelta))^2$ (w as given in the right hand side of Eq. (2)) at all digitized data points with respect to the unknown coefficients $A_0 (\propto K_{\mathrm{Id}})$, A_1 and A_2 the SIF was evaluated.

4. Numerical simulations

4.1. Elasto-static computations

Companion finite element simulations of cracked FGM samples were carried out. *Plane stress* elasto-static simulations of cracked beams subjected to pure bending were performed for both FGMs and homogeneous materials. Owing to the symmetry, only one half of the beam was modeled with appropriate force and displacement boundary conditions. In the case of FGM beams, measured Young's modulus gradient from the samples was prescribed for FGMs using a novel technique developed by Rousseau and

Tippur [16]. The method essentially consists of a two step process in which first a thermo-mechanical problem is solved with a temperature distribution that corresponds to the required Young's modulus gradient to be imposed and coefficient of linear expansion set equal to zero over the entire domain. In the second step, Young's modulus is described as a function of the temperature gradient and the mechanical problem is solved. The Poisson's ratio was assumed constant and equal to a value corresponding to that of the crack tip, throughout the model. Separate simulations were carried out for situations with crack located on the stiff and the compliant sides of FGM beams. The corresponding crack tip elastic properties were used in separate homogeneous beam simulations. A typical model consisted of 8600 eight-noded iso-parametric elements with 26 000 nodes and two degrees of freedom per node, as shown in Fig. 5. The crack tip region had a square mesh with a typical size of 50–100 μm.

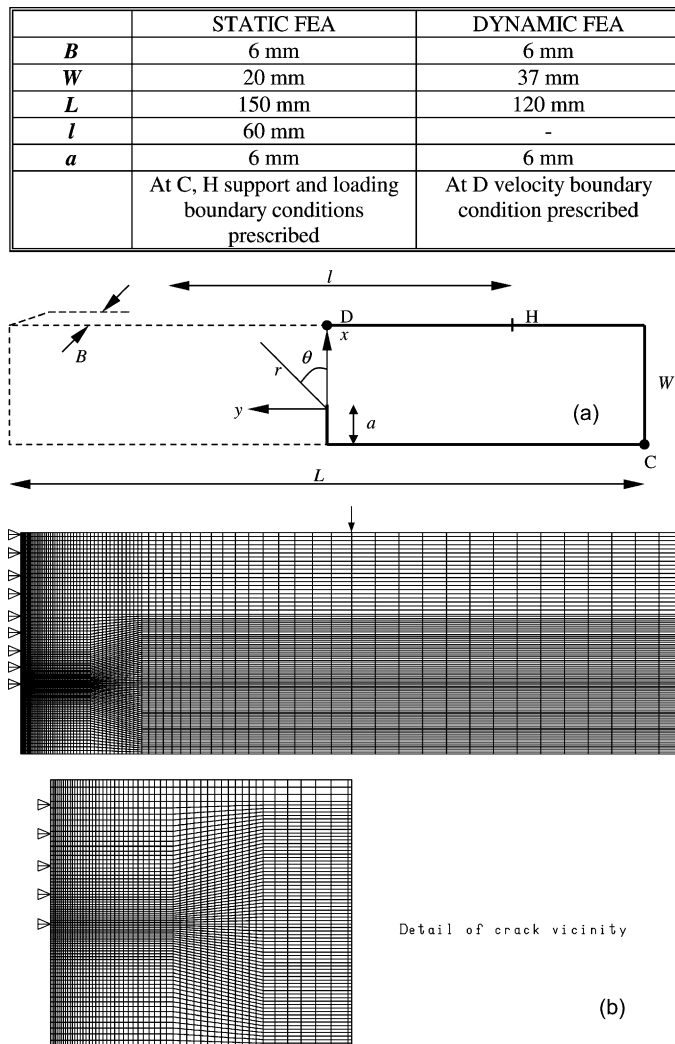|	STATIC FEA	DYNAMIC FEA
B	6 mm	6 mm
W	20 mm	37 mm
L	150 mm	120 mm
l	60 mm	-
a	6 mm	6 mm
	At C, H support and loading boundary conditions prescribed	At D velocity boundary condition prescribed

Fig. 5. Schematic of the geometry and loading configurations used in FEA models (a). Typical FGM finite element mesh (b).

In the immediate vicinity of the crack tip, assuming K-dominance, the expressions for crack opening displacements were truncated to the leading term and used for determining SIFs in FGMs in the limit $r \rightarrow 0$. Thus, for a locally homogeneous material behavior, crack opening displacement for an FGM is,

$$\delta_y(t)|_{\theta=\pm\pi, r\rightarrow 0} = \frac{8\overline{K}_{\mathrm{I}}(t)}{E_0} \sqrt{\frac{r}{2\pi}}. \tag{7}$$

Here, E_0 is the crack tip Young's modulus. The variation of $\overline{K}_{\mathrm{I}}(r, \pm\pi)$ obtained from the finite element solution was first plotted and its extrapolated value at the crack tip was identified as the SIF:

$$K_{\mathrm{I}} = \lim_{r\rightarrow 0} \overline{K}_{\mathrm{I}}. \tag{8}$$

4.2. Elasto-dynamic computations

Companion *plane stress* elasto-dynamic finite element simulation of all the three categories of experiments, homogeneous and the two FGMs, were performed. A two-dimensional quadrilateral mesh of eight-noded isoparametric elements with two degrees of freedom per node was used in the analysis. Again because of the symmetry, only one half of each sample was modeled, with approximately 10000 nodes and 3300 elements. The crack tip vicinity was highly refined as in static simulations for accurate evaluation of crack tip parameters. (The model was first benchmarked against elasto-dynamic finite element results for a mixed-mode stationary crack problem in homogeneous material. The details are avoided here for brevity.) Simulations were conducted as a one-point symmetric impact of an elastic planar medium by a rigid impactor, by imposing the downward velocity of 5.3 m/s (equal to the impact velocity of the experiments) to the topmost node in the plane of the crack. The Newmark time-integration scheme was used with a minimum time step of 0.04 μs. As in the static simulations, instantaneous mode-I SIFs were determined by regression analysis of crack tip opening displacements at discrete time intervals of every 5 μs after impact until crack initiation.

5. Results and discussion

5.1. Static loading

FGM specimens were subjected to far-field bending stress ($6M/BW^2$) of 10.2 MPa. The FGM sample with a crack located on its compliant side had a crack tip modulus $E_0 = 4.8$ GPa, and a modulus ratio (E_2/E_1) between its two edges of 2.2. The other FGM sample, with an edge crack on the stiff side had a crack tip modulus $E_0 = 6.8$ GPa, and a modulus ratio of 0.4. The homogeneous samples with moduli corresponding to those at the crack tips (E_0) of the FGMs were subjected to far-field stresses identical to those of their FGM counterparts, so that a direct comparison could be made.

A comparison of the mode-I SIFs obtained from the analysis of interferograms is presented in Table 1. Under the premise of K-dominance, the experimental values of K_{I} for the FGMs are about 20% lower than those predicted by the finite element calculations. When least-squares analysis including nonsingular contributions to the singular field was carried out with two terms of the expansion field (Eq. (5)), the values of SIFs improved and the error between the numerical and experimental results reduced to 10% or less.

The influence of elastic gradient on statically loaded FGM beams can be inferred from SIF results. The beam with a crack on the glass-rich (stiff) side ($E_2/E_1 < 1$) experience higher value of K_{I} when compared to its homogeneous counterpart subjected to identical far-field loading. On the other hand, the FGM beam with a crack on the epoxy-rich (compliant) side ($E_2/E_1 > 1$) of the beam experiences a lower K_{I} compared to

Table 1
Comparison of computed and measured SIFs for a static far-field bending stress $(6M/BW^2) = 10.2$ MPa

Method of calculation	FGM $E_2/E_1 = 2.23$, $E_0 = 4.8$ GPa	Homogeneous $E_2/E_1 = 1$, $E_0 = 4.8$ GPa	FGM $E_2/E_1 = 0.41$, $E_0 = 6.8$ GPa	Homogeneous $E_2/E_1 = 1$, $E_0 = 6.8$ GPa
FEA (plane stress)	1.27	1.51	1.77	1.45
Optically measured (K-dominant description)	1.06	1.26	1.44	1.20
Optically measured (asymptotic expansion)	1.13	1.44	1.80	1.50

its homogeneous counterpart. Thus in the specific case studied, the results suggest that elastic gradients shield a crack on the compliant side and lower the SIF by a factor of about 1.5 when compared to the one with the crack on the stiff side.

5.2. Dynamic loading

Instantaneous SIFs, $K_{Id}(t)$, were evaluated up to crack initiation. Symbols in Fig. 6(a) and (b) represent optically determined dynamic stress factor history for the two FGMs with $E_2/E_1 < 1$ and $E_2/E_1 > 1$, respectively. In these plots, time after impact is normalized with respect to the dilatational wave speed at the crack tip location and the specimen height: $T = tC_l W$. Finite element results are also plotted as a solid line, up to crack initiation, t_I (determined experimentally). Good agreement between the two is evident. Note the absence of experimental data points for certain frames because of either loss of optical information and/or, during early stages of fringe formation, the fringes reside within the region of dominant triaxiality where they can not be reliably analyzed.

For comparison purposes, normalized SIFs are plotted against normalized time for the two FGMs and homogeneous sample in Fig. 6(c). In this plot, SIFs are normalized by the corresponding value at initiation. In each case, monotonic increase in $K_{Id}(t)$ is observed. Crack initiation occurred at $T \sim 6.8$ after initiation for the homogeneous material. Evidence of crack motion was not observed until $T \sim 6.2$ and 7.2 for the FGMs with $E_2/E_1 > 1$ and $E_2/E_1 < 1$, respectively. Note that the behavior of the homogeneous material lies between those of the two FGMs. Interestingly, crack initiation in FGMs with $E_2/E_1 < 1$ are delayed relative to the opposite FGM configuration and the homogeneous sample. Also, evident from the plots are
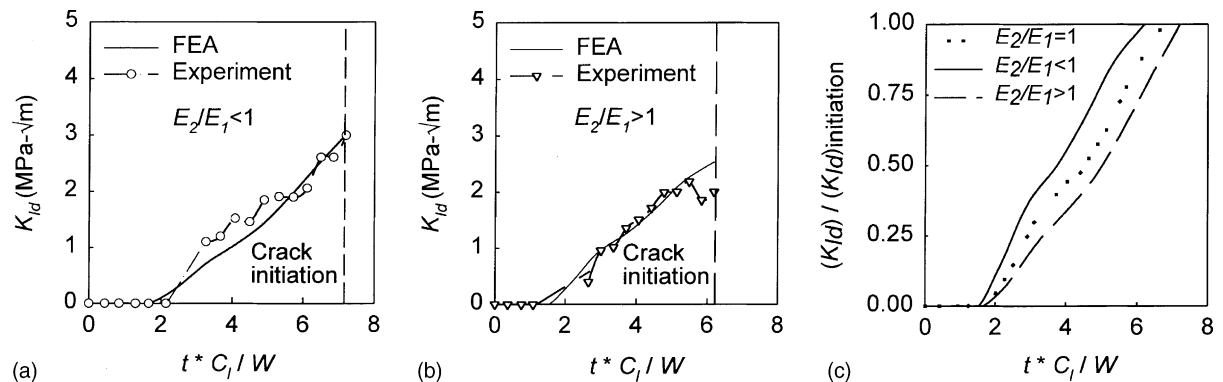

Fig. 6. Measured mode-I dynamic SIF history compared with FEA for FGM with $E_2/E_1 < 1$ (a), $E_2/E_1 > 1$ (b). Normalized SIF for FGMs and homogeneous materials (c).

the differences in the crack tip loading rate ($\Delta K_{\text{Id}}/\Delta t$) with lower rate seen in case of the FGM with the crack on the stiff side of the beam.

In the results discussed above, in addition to the local fracture toughness difference at the crack tips, it should be noted that crack initiation event is affected by combination of differences in the average values of wave speeds, crack tip elastic modulus and crack tip elastic gradients ($\mathrm{d}(E/\rho)/\mathrm{d}X$) between samples. Accordingly finite element simulations were carried out to isolate the effect of elastic gradients on crack initiation. Homogeneous beams and FGM beams with assumed linear elastic variations were simulated. Further, material variations were identified in terms of E/ρ variations and Poisson's ratio was kept constant ($\nu = 0.34$). Material properties implemented were close to those realized in the actual glass/epoxy FGMs used in the experiments. The Young's moduli were varied between 4 and 12 GPa, and densities between 950 and 1850 kg/m^3. Individual variations of E and ρ were implemented using a 'look-up' chart relating E, ρ, (and E/ρ) to filler volume fraction in actual glass-filled epoxy. The prescribed elastic gradients consisted of linearly increasing and decreasing values of E/ρ for FGMs, and constant E/ρ representing homogeneous materials, all having identical properties at he crack tip (Fig. 7(a)). By selecting an $a/W = 0.5$, the crack tip Young's moduli, average value of the elastic wave speeds and $|\mathrm{d}(E/\rho)/\mathrm{d}X|$ were identical in all three situations. Thus, the influence of increasing and decreasing elastic gradients could be isolated.

Plot of K_{Id} history after impact is shown in Fig. 7(b) for the three cases. The variation in SIF for the FGM with $E_2/E_1 > 1$ displays the highest rate of increase whereas the FGM with $E_2/E_1 < 1$ has the lowest rate of increase. The homogeneous material response lies in between the two FGMs. Rates of increase in $\mathrm{d}K_{\text{Id}}/\mathrm{d}t$ (Fig. 7(c)) are also lowest for FGM with $E_2/E_1 < 1$, followed by the homogeneous material. The FGM with $E_2/E_1 > 1$ has the steepest increase up to $T \sim 5$. Beyond that point, an inflection in the curve drops the increase in stress intensification below that of the homogeneous material but still higher than that for FGM with $E_2/E_1 < 1$. Material properties at the crack tip being the same in all the three cases, for an *assumed* critical value of SIF of, say, 3 MPa $\sqrt{\text{m}}$, crack initiation occurs (Fig. 7(b)) at $T \sim 5.8$, 6.6, and 7.9 for FGM with increasing gradient, homogeneous material, and FGM with decreasing gradient, respectively. These trends are identical to the ones observed experimentally. Thus, purely based on elastic considerations, crack initiation in the latter case is significantly delayed, by a factor of ~ 1.4, when compared to the former. Behavior of the homogeneous material, as with all other parameters, lies between the two FGMs.

To further understand these differences, additional dynamic impact simulations on *uncracked* beams (FGM and homogeneous) were performed for monitoring stress histories. Contours of $(\sigma_x + \sigma_y)$ for all
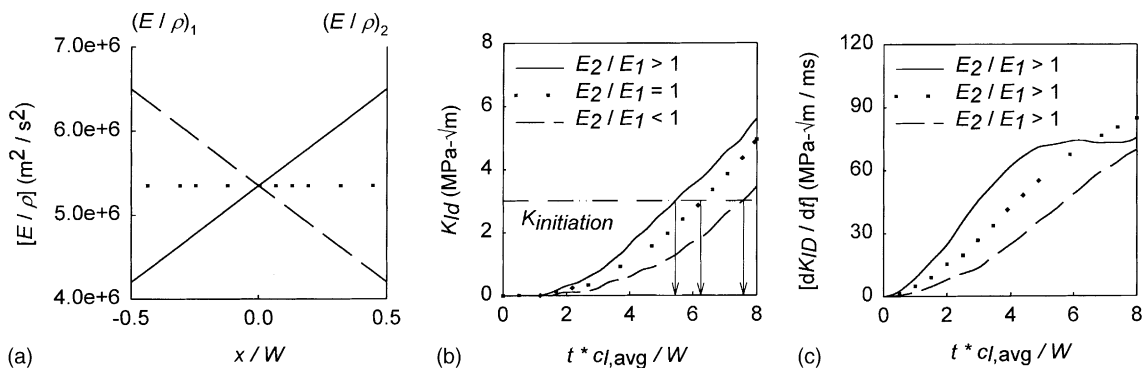

Fig. 7. SIF history in homogeneous beams and FGMs with linearly varying gradients (crack tip located at $X/W = 0.5$ or $x/W = 0$). (a) Elastic variations used in the FEA, (b) SIF histories, and (c) crack tip loading rate histories (W = height of the sample).
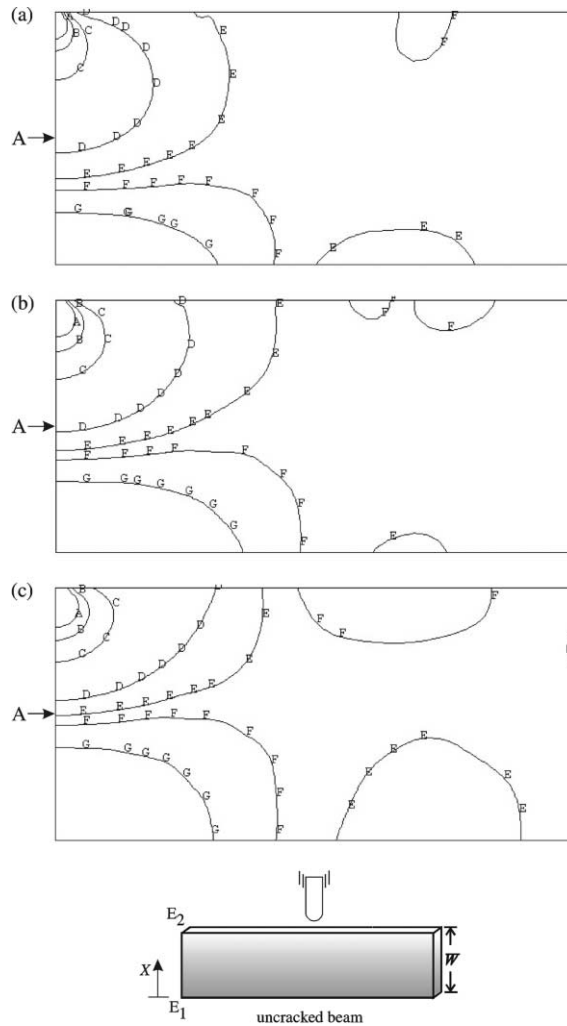
Fig. 8. $(\sigma_x + \sigma_y)$ contours at nondimensional time $T = 5.7$ ($A = -5$, $B = -3.5$, $C = -2$, $D = -0.5$, $E = -0.1$, $F = 0.1$, $G = 0.5$) $*$ 10 MPa. (a) $E_2/E_1 < 1$, (b) $E_2/E_1 = 1$, $E_2/E_1 > 1$. Point A corresponds to $(X/W = 0.5, y = 0)$. Note that only the right-half of the beam is modeled.

three materials are shown in Fig. 8 after several wave reflections ($T = 5.7$) between the top and bottom edges. Relative to the homogeneous beam (Fig. 8(b)), compressive waves emanating from the impact point for the FGM with $E_2/E_1 > 1$ (Fig. 8(c)) are constricted vertically, whereas those for the FGM with $E_2/E_1 < 1$ (Fig. 8(a)) are elongated in the same direction. In the former case, as compressive waves (for example, contour level D) travel from the top to the bottom edge, they are delayed by material property variations in that direction. Conversely, for the FGM with $E_2/E_1 < 1$, material property variation promotes faster wave propagation downwards, thereby elongation of $(\sigma_x + \sigma_y)$ contour (again, level D) along the beam height is evident. The reflected tensile waves accelerate upward for FGMs with $E_2/E_1 > 1$, decelerate for FGMs with $E_2/E_1 < 1$, and propagate at a constant speed in the homogeneous case. As seen in Fig. 8, at time $T = 5.7$, a point A (located at $X/W = 0.5$) along the line of symmetry of the beam experiences tensile stresses for the FGM with $E_2/E_1 > 1$ while the corresponding points in the homogeneous

beam and the FGM beam with $E_2/E_1 < 1$ experience progressively higher compressive stresses, respectively. Accordingly, the latter two cases are elastically shielded from tensile stresses for a longer duration and would experience delayed crack initiation.

6. Concluding remarks

Influence of elastic variations on crack initiation in compositionally graded beams was studied experimentally and numerically. Beam samples with unidirectional elastic gradients subjected to static four-point bending and dynamic one-point impact loading were considered for experimentation. Compositionally graded epoxy with solid-microsphere glass filler was the material of choice for producing elastic gradients by continuously varying filler volume fractions over the height of the beam samples. Macroscopic Young's modulus variations of about 1:3 and density of about 1:2 were realized using gravity casting. The optical method CGS was used for measuring surface slopes in the direction of elastic gradients. The high-speed photography was utilized for dynamic crack initiation studies for capturing instantaneous deformation field histories. A locally homogeneous material behavior in the immediate vicinity of the FGM crack tip is assumed for extracting SIFs in both static and dynamic situations using continuum models for crack stresses. Companion plane stress finite element simulations for both static and dynamic loading situations were performed and SIFs were determined using regression analysis of crack tip opening displacements. The experimentally determined values of SIFs are in good agreement with the ones from computations.

Under static loading conditions, the elastic gradients offer crack tip shielding. In the specific examples studied, the crack tip located on the compliant side of a beam subjected to pure bending moment experienced SIF 1.5 times lower than that with a crack on the stiff side in a beam with an identical elastic variation. In the dynamic experiments, crack initiation in situation when the crack is located on the stiffer side of the beam were delayed when compared to the opposite situation when the crack is located on the compliant. However, this was a combined effect of the crack tip variables such as elastic properties, elastic gradient and the local fracture toughness. Accordingly, computations on dynamically loaded stationary cracks were performed for idealized situations where identical crack tip elastic properties were enforced and the effect of elastic gradients alone was isolated. Results confirmed the experimental observation that crack initiation in an FGM with crack on the stiff side of a beam subjected to symmetric one-point impact is delayed considerably when compared to the opposite configuration due to lower rate of crack tip loading.

Acknowledgements

References

[1] Nino M, Hirai T, Watanabe R. The functionally gradient materials. J Jpn Soc Compos Mater 1987;13:257.
[2] Atkinson C, List RD. Steady state crack propagation into media with spatially varying elastic properties. Int J Eng Sci 1978;16:717–30.
[3] Delale F, Erdogan F. The crack problem for a nonhomogeneous plane. ASME J Appl Mech 1983;50:609–14.
[4] Eischen JW. Fracture of nonhomogeneous materials. Int J Fract 1987;34:3–22.
[5] Jin Z-H, Noda N. Crack-tip singular fields in nonhomogeneous materials. ASME J Appl Mech 1994;61:738–40.
[6] Erdogan F. Fracture mechanics of functionally graded materials. Compos Eng 1995;7:753–70.

[7] Babaei R, Lukasiewicz SA. Dynamic response of a crack in a functionally graded material between two dissimilar half-planes under anti-plane shear impact load. Eng Fract Mech 1998;60:479–87.

[8] Nakagaki M, Wu YD, Hagihara S. Dynamically propagating crack in graded particle dispersed composites. Fract Strength Sol 1998;145:333–42.

[9] Parameswaran V, Shukla A. Dynamic fracture of a functionally gradient material having discrete property variation. J Mater Sci 1998;33:3303–11.

[10] Chiu TC, Erdogan F. One-dimensional wave propagation in a functionally graded elastic medium. J Sound Vib 1999;222:453–87.

[11] Marur PR, Tippur HV. Evaluation of mechanical properties of functionally graded materials. J Testing and Evaluation 1998;26:539–45.

[12] Butcher RJ, Rousseau C-E, Tippur HV. A functionally graded particulate composite: preparation measurements and failure analysis. Acta Mater 1999;47:259–68.

[13] Parameswaran V, Shukla A. Processing and characterization of a model functionally gradient Material. J Mater Sci 2000;35:21–9.

[14] Li H, Lambros J, Cheeseman B, Santare MH. Experimental investigation of quasi-static fracture of functionally graded material. Int J Solids Struct 1999;37:3715–32.

[15] Marur PR, Tippur HV. Dynamic response of bimaterial and graded interface cracks under impact loading. Int J Fract 2000;103:103–9.

[16] Rousseau C-E, Tippur HV. Compositionally graded materials with cracks normal to the elastic gradient: examination of fracture parameters relative to bimaterials. Acta Mater 2000;48:4021–33.

[17] Rousseau C-E. Evaluation of crack tip fields and fracture parameters in functionally graded materials. PhD Dissertation, Auburn University, 2000.

[18] Weng GJ. Some elastic properties of reinforced solids with special reference to isotropic ones containing spherical inclusions. Int J Eng Sci 1984;22:845–56.

[19] Tippur HV, Krishnaswamy S, Rosakis AJ. A coherent gradient sensor for crack tip deformation measurements: analysis and experimental results. Int J Fract 1991;48:193–204.

[20] Rosakis AJ, Ravi-Chandar K. On crack-tip stress state: an experimental evaluation of three-dimensional effects. Int J Solids Struct 1986;22:121–38.

[21] Sinha JK, Tippur HV, Xu L. An interferometric and finite element investigation of interfacial crack tip fields: role of mode-mixity on 3D stress variation. Int J Solids Struct 1997;34:741–54.